ACS Chemical Neuroscience

Research Article

pubs.acs.org/chemneuro

Alpha-Synuclein Regulates Neuronal Levels of Manganese and Calcium

Tanja Dučić,[*,†,▽] Eleonora Carboni,[§,∥,▽] Barry Lai,[‡] Si Chen,[‡] Bernhard Michalke,[⊥] Diana F. Lázaro,[#] Tiago F. Outeiro,[#] Mathias Bähr,[§,∥] Elisabeth Barski,[§] and Paul Lingor[*,§,∥]

[†]CELLS − ALBA, Carretera BP 1413, de Cerdanyola del Vallès a Sant Cugat del Vallè, km. 33, 08290 Cerdanyola del Vallès, Barcelona, Spain

[‡]Advanced Photon Source, Argonne National Laboratory, 9700 S. Cass Avenue, Argonne, Illinois 60439, United States,

[§]Department of Neurology, University Medicine Göttingen, Robert-Koch-Str. 40, 37075 Göttingen, Germany

[∥]DFG-Research Center for Nanoscale Microscopy and Molecular Physiology of the Brain, 37073 Göttingen, Germany

[⊥]Helmholtz Zentrum München, Ingolstädter Landstr. 1, 85764 Neuherberg, Germany

[#]Department of Neurodegeneration and Restorative Research, University Medicine Göttingen, Waldweg 33, 37073 Göttingen, Germany

Supporting Information

ABSTRACT: Manganese (Mn) may foster aggregation of alpha-synuclein (αSyn) contributing to the pathogenesis of PD. Here, we examined the influence of αSyn overexpression on distribution and oxidation states of Mn in frozen-hydrated primary midbrain neurons (PMNs) by synchrotron-based X-ray fluorescence (XRF) and X-ray absorption near edge structure spectroscopy (XANES). Overexpression of αSyn increased intracellular Mn levels, whereas levels of Ca, Zn, K, P, and S were significantly decreased. Mn oxidation states were not altered. A strong correlation between Cu-/Mn-levels as well as Fe-/Mn-levels was observed in αSyn-overexpressing cells. Subcellular resolution revealed a punctate or filament-like perinuclear and neuritic distribution of Mn, which resembled the expression of DMT1 and MnSOD. While overexpression of αSyn did not significantly alter the expression patterns of the most-expressed Mn transport proteins (DMT1, VGCC, Fpn1), it attenuated the Mn release from Mn-treated neurons. Thus, these data suggest that αSyn may act as an intracellular Mn store. In total, neurotoxicity in PD could be mediated via regulation of transition metal levels and the metal-binding capacity of αSyn, which could represent a promising therapeutic target for this neurodegenerative disorder.

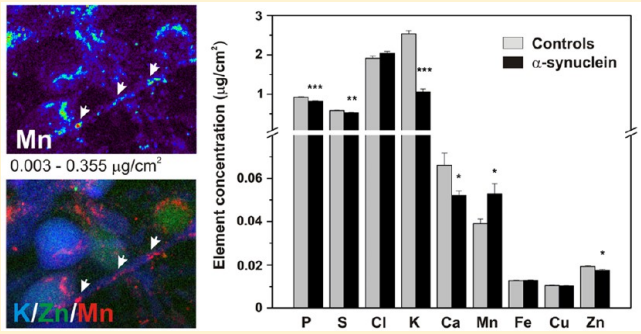

KEYWORDS: *X-ray fluorescence, XANES spectroscopy, alpha-synuclein, manganese, calcium*

Manganese (Mn) is an essential element required in trace amounts for proper cell function. It is a cofactor of several enzymes like pyruvate carboxylase, arginase, serine/threonine glutamine synthase, and mitochondrial superoxide dismutase.[1] Despite its vital role in enzymatic reactions, excessive Mn exposure can induce a neurological syndrome known as manganism, resulting in rigidity and/or dystonia.[2] This syndrome is associated with loss of dopamine in the striatum and death of neurons in the striatum and globus pallidus,[3] thus sharing several features with idiopathic Parkinson's disease (PD).

PD is the second most frequent neurodegenerative disease with symptoms such as rigidity, tremor and bradykinesia.[4,5] Its pathological characteristics include the preferential, but not exclusive loss of dopaminergic neurons within the substantia nigra pars compacta and the presence of intracytoplasmic inclusions, Lewy bodies, whose primary components include fibrillar α-synuclein (αSyn). Although αSyn in idiopathic PD occurs in its wild-type form, several mutations of the protein are known, which result in familial PD.[6] More interestingly, not only mutations, but also duplications and triplications of the αSyn gene result in phenotypic PD, suggesting a dosage effect of the protein.[7] A number of recent studies have shown that αSyn interacts with transition metals, such as Mn, Fe, Cu, and Zn and these interactions can lead to protein aggregation and cross-linking.[8,9] Nevertheless, questions still arise as to whether these in vitro observations are physiologically relevant. It is also unknown if and how increased levels of αSyn regulate intracellular levels of transition metals.

In addition to the total amount, the valence of metal ions plays a key role in their cellular toxicity. For example, Mn

Received: March 20, 2015
Revised: July 30, 2015
Published: August 18, 2015

DOI: 10.1021/acschemneuro.5b00093
ACS Chem. Neurosci. 2015, 6, 1769−1779

toxicity is conferred by oxidation of important cellular components by Mn^{3+}.[10] The amount of Mn^{3+} in neuronal cells can thus be indicative for the extent of oxidative damage induced by Mn^{3+}.

In order to better understand the interplay of αSyn and Mn, we evaluated Mn-treated rat primary midbrain neurons (PMNs) overexpressing αSyn as a cellular model of PD with X-ray fluorescence (XRF) imaging methods in this study. To be able to detect elemental changes in situ at highest sensitivity and spatial resolution,[11] we used a synchrotron-based X-ray microscope, the Bionanoprobe (BNP) at the Advanced Photon Source (APS, Argonne, IL), which has the ability to operate in a cryo-environment, preserving samples at the closest-possible to native physiological conditions, especially regarding to the location and concentration of fast diffusible elements. This technique also allows visualizing entire intact cells without the need for chemical fixation or sectioning.[12] After precise elemental mapping, the X-ray absorption near edge structure spectroscopy (XANES) was employed to determine the oxidation states of manganese within the cells in situ at beamline 2-ID-D at the APS. The aim of our study was to analyze whether and how spatial distribution and concentration of Mn and other elements depend on αSyn levels in PMNs. We show that overexpression of αSyn is a significant modulator of Mn as well as Ca levels and additionally alters the distribution of other elements suggesting detrimental effects on whole cellular metabolism.

RESULTS

Elemental Distribution in Untreated Control Cultures. For an assessment of baseline elemental distribution, cryopreserved midbrain cultures, which did not undergo treatment with Mn, were imaged (Figure 1). Twelve independent cells were studied in detail. Only low concentrations of Ca (0.051 ± 0.007 $\mu g/cm^2$) and Mn (0.0014 ± 0.0001 $\mu g/cm^2$) were measured in control cultures. No compartment-specific distribution of Mn was detected. The distribution of K, S, and P was used to define the morphology of the neurons (Figure 1).

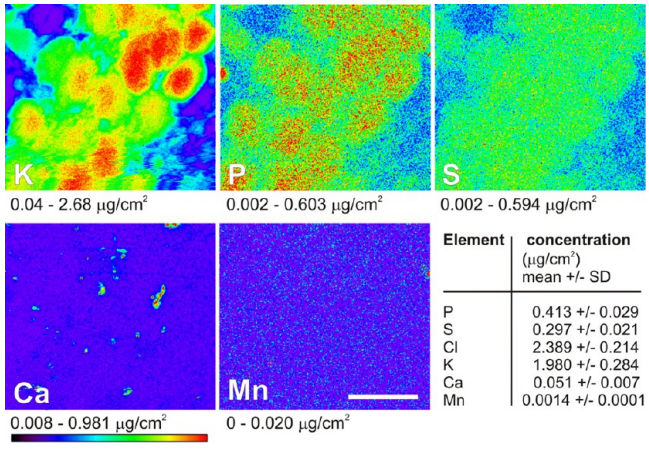

Figure 1. Elemental maps of control primary midbrain neurons. X-ray fluorescence images of K, P, S, Ca, and Mn maps measured at photon energy 6.57 keV. Image size 60 × 55 μm^2, pixel size 250 nm, dwell time 300 ms. Rainbow color scale corresponds to elemental concentrations in the range given below each map. Mean elemental concentrations for single cells in $\mu g/cm^2$ are given in the table (n = 12). Scale bar: 20 μm.

Overall Elemental Concentrations in Midbrain Neurons. In order to examine the overall elemental content of αSyn-overexpressing and control midbrain neurons after Mn treatment, we obtained larger overview images. These images contained numerous αSyn-transfected and nontransfected neurons for a quantitative analysis on a sufficiently large number of cells permitting robust statistical evaluation (Figure 2). We quantified the X-ray fluorescence images of 18 cells

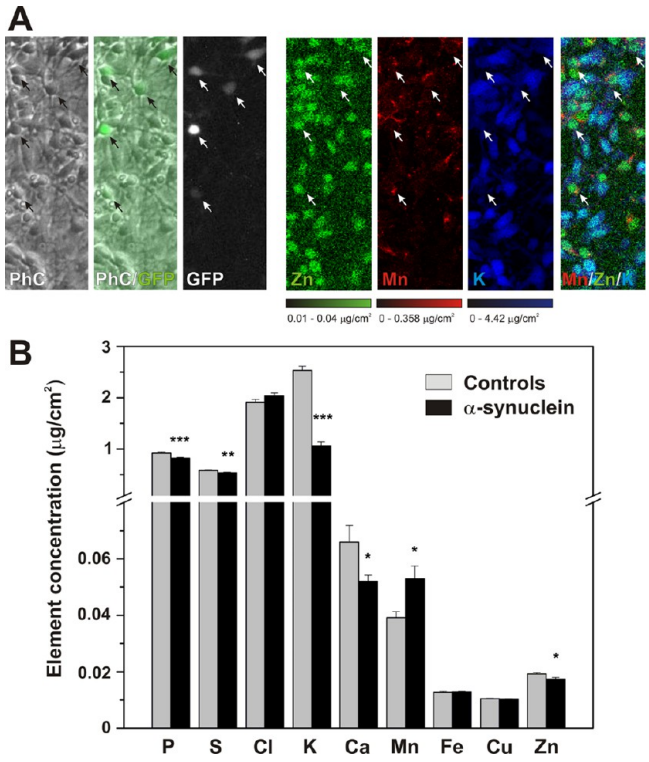

Figure 2. Quantification of elemental concentrations in alpha-synuclein overexpressing neurons and controls. (A) Representative photomicrographs of the primary midbrain neuron culture treated with 500 μM Mn^{2+}. Phase contrast image (PhC), GFP fluorescence representing neurons overexpressing αSyn (GFP) and merged image (PhC/GFP). X-ray fluorescence maps show the same cells culture area imaged at cryogenic conditions at photon energy of 10 keV: Zn (green), Mn (red), K (blue), and a merged map of Zn, Mn, and K are shown. Image size 240 × 81 μm^2, pixel size 1 μm, dwell time 250 ms. Color scales correspond to elemental concentrations in the ranges given below each map. Arrows point to GFP-positive (αSyn-overexpressing) neurons. (B) Diagram summarizing elemental concentrations in control neurons (n = 40; gray bars) and αSyn-overexpressing neurons (n = 18; black bars) in $\mu g/cm^2$. Values are given as means ± SE. *P < 0.05; **P < 0.01; ***P < 0.001 according to two-sided Student's t test.

overexpressing αSyn and 40 control cells. The elemental concentrations for P, S, Ca, K, and Zn were significantly decreased, while Mn concentration were significantly elevated in neurons overexpressing αSyn in comparison to control cells (P: 0.818 ± 0.082 vs 0.919 ± 0.114 $\mu g/cm^2$; S: 0.531 ± 0.058 vs 0.585 ± 0.060 $\mu g/cm^2$; Ca: 0.052 ± 0.009 vs 0.066 ± 0.037 $\mu g/cm^2$; K: 1.06 ± 0.34 vs 2.53 ± 0.50 $\mu g/cm^2$; Zn: 0.017 ± 0.002 vs 0.019 ± 0.003 $\mu g/cm^2$; and Mn: 0.053 ± 0.019 vs 0.039 ± 0.013 $\mu g/cm^2$, respectively). The concentrations of Cl, Cu, and Fe did not significantly differ in the two groups (Figure 2).

DOI: 10.1021/acschemneuro.5b00093
ACS Chem. Neurosci. 2015, 6, 1769−1779

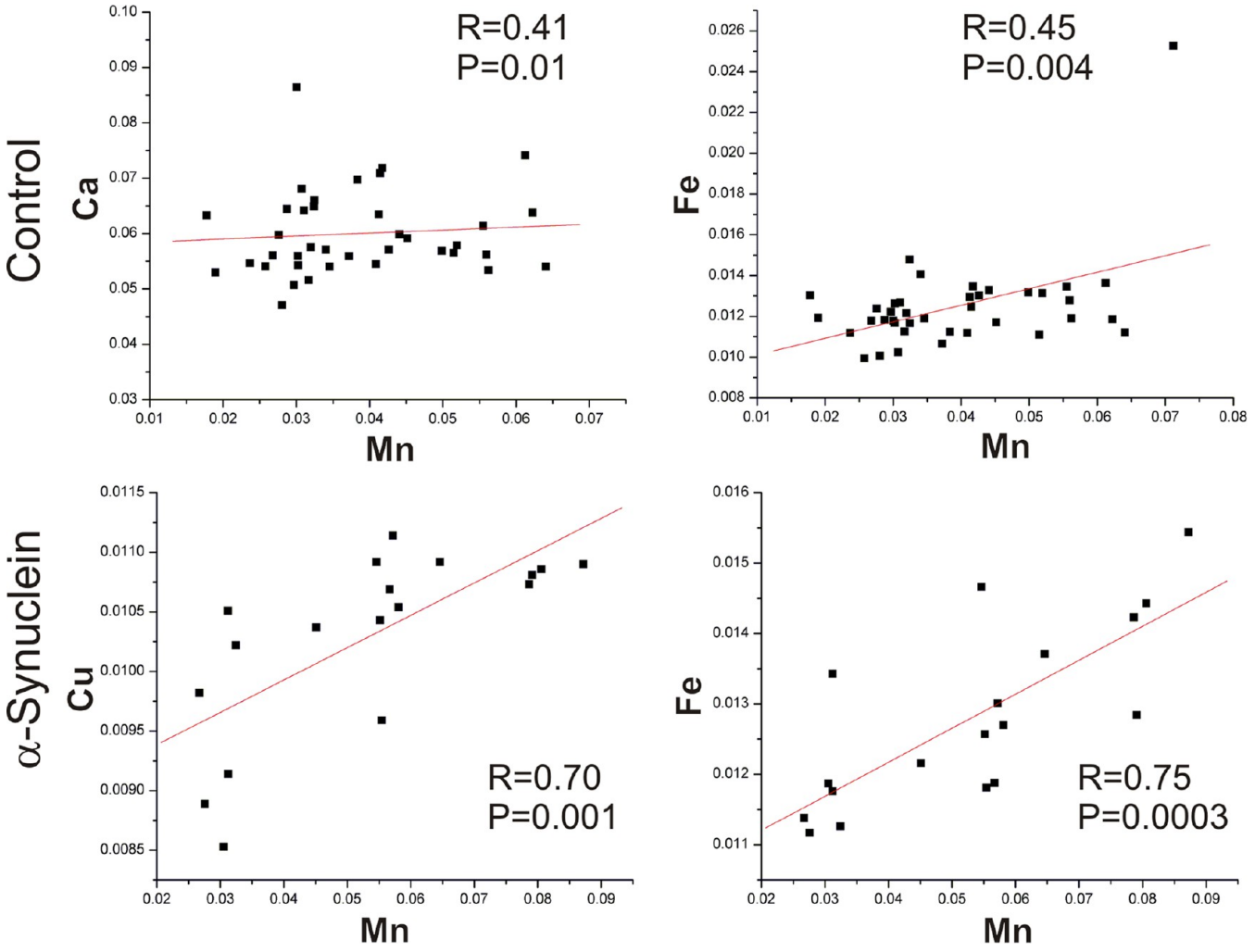

Figure 3. Correlation plots of intracellular elemental concentrations. Control neurons (n = 40) show a significant correlation between concentrations of Mn and Ca as well as Mn and Fe. Neurons overexpressing αSyn (n = 18) show strong correlation between Mn and Cu as well as Mn and Fe. The Pearson's correlation coefficients (R) and p-values are given for each plot.

To analyze whether relationships existed among different element concentrations, correlation analyses were performed (Figure 3). In control neurons, we found only a weak positive correlation between Mn and Ca concentrations (R = 0.41; p = 0.01) and between Mn and Fe concentrations (R = 0.45; p = 0.004), (Figure 3), and a stronger correlation between Ca and Fe (R = 0.84 and $p = 1 \times 10^{-11}$, data not shown). Interestingly, in αSyn-overexpressing cells, a strong correlation between Mn and Fe concentrations (R = 0.75; p = 0.0003) and Mn and Cu concentrations (R = 0.70; p = 0.001) was observed (Figure 3). Between Cu and Fe, the Pearson's correlation coefficient R was 0.54 (p = 0.02) (not shown).

Subcellular Elemental Quantification. After determination of the overall elemental concentration in primary midbrain neurons, we now focused in more detail on the subcellular distribution of selected elements. Our aim was to analyze whether transfection with αSyn alters elements distribution and therefore could yield additional information on the pathophysiological function of this protein.

Potassium and sulfur maps were used for the cellular orientation. Sulfur as a protein marker is present in the amino acids methionine and cysteine and is therefore distributed throughout the cell in all cellular proteins.[13] The Zn signal can be used as a proxy for the general size of the nucleus, as Zn content has been shown to be elevated in the nucleus.[14,15] In native neuronal cells, which were not overexpressing αSyn, Mn was distributed in a nonhomogeneous, patchy pattern, concentrating in specific areas, projecting mostly to the perinuclear space and less to the nucleus itself (Figure 4, Mn). The maximum concentration of Mn in these spots, not larger than ∼1 μm in diameter, reached 215 ng/cm^2. In some areas Ca distribution was overlapping with Mn. Interestingly, Fe was observed in the same perinuclear cytoplasmic compartment as Mn and there was some colocalization of both metals (marked with white arrows in Figure 4).

In contrast, primary neurons overexpressing αSyn showed a more compartmentalized distribution of Mn that was clearly localized around the signal for Zn, which is indicative of the nucleus (Figure 5). Similarly to control neurons, a prominent colocalization of Mn with Fe was observed (Figure 5). Next to cell somata, Mn was also localized in neurites (Figure 6). Also here, the distribution of Mn was not homogeneous, but followed a patchy structure projecting on to the neurites (Figure 6). Because overexpression of αSyn did not result in formation of inclusions in our experimental paradigm (Supporting Information Figures S1 and S3), the intracellular Mn accumulations cannot be attributed to binding of Mn to αSyn inclusions. Therefore, we compared the distribution of

DOI: 10.1021/acschemneuro.5b00093
ACS Chem. Neurosci. 2015, 6, 1769−1779

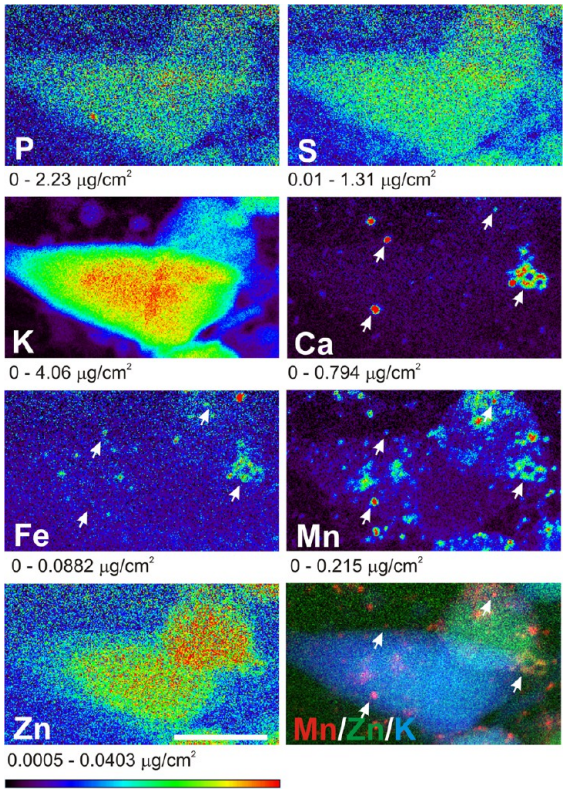

Figure 4. Elemental maps of control primary midbrain neurons treated with 500 μM Mn^{2+}. Representative XRF elemental maps of P, S, K, Ca, Fe, Mn, Zn, and a merged map of Mn/Zn/K imaged at cryogenic conditions by using photon energy of 10 keV. Arrows point to Mn-rich areas, partially enriched in Ca and/or Fe. Image size 29 × 17 μm^2, pixel size 100 nm, dwell time 250 ms. Rainbow scale corresponds to elemental concentrations in the ranges given below each scan. Scale bar: 10 μm.

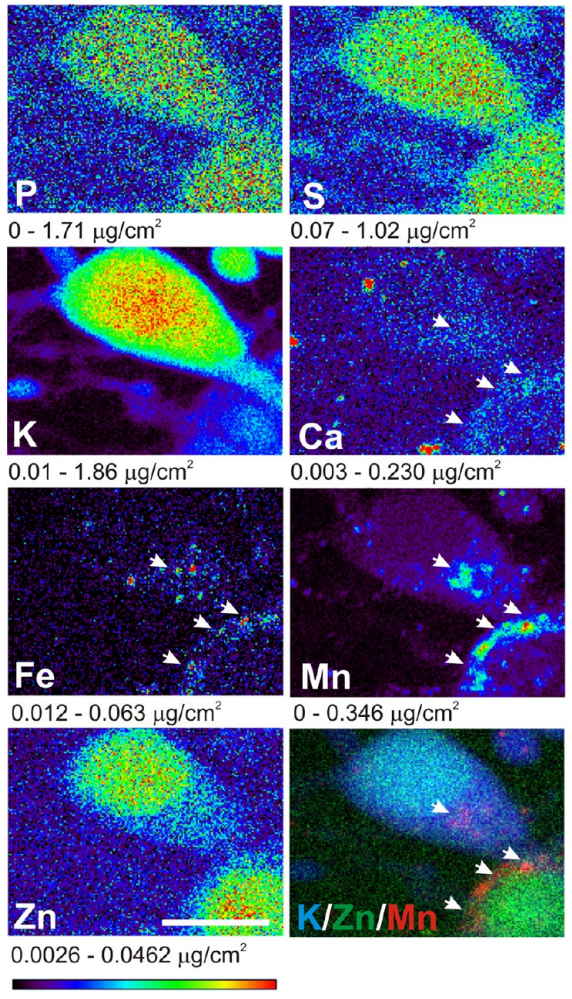

Figure 5. Elemental maps of primary midbrain neurons overexpressing αSyn treated with 500 μM Mn^{2+}. Representative XRF elemental maps of P, S, K, Ca, Fe, Mn, Zn, and a merged map of Mn/Zn/K imaged at cryogenic conditions and photon energy of 10 keV. Arrows point to Mn-rich areas, which partially are also enriched in Ca and/or Fe. Image size 25 × 19 μm^2, pixel size 150 nm, dwell time 250 ms. Rainbow scale corresponds to elemental concentrations in the ranges given below each scan. Scale bar: 10 μm.

Mn visualized by X-ray fluorescence with the expression of two important Mn-related proteins, MnSOD and DMT1. While DMT1 is the main Mn importer in the cell and is located in the membrane and in organelles, MnSOD is a major detoxifying enzyme for reactive oxygen species and is located mainly in the mitochondria.[16] Immunocytochemistry for DMT1 revealed a rather punctate to patchy distribution in the somatic cytoplasm and also in the neurites, possibly representing organelles (Figure 7A–C). In contrast, MnSOD presented both in the cytoplasm and in neurites rather as elongated, filament-like structure colocalizing with the mitochondrial marker TOM20 (Figure 7D–F). Both of these patterns resembled the distribution of Mn observed by high-resolution imaging: the punctate/patchy structure of DMT1 strongly resembled the distribution of Mn observed by X-ray flurescence in Figures 4 and 5, while the more filament-like localization of Mn in Figure 6 resembled that of TOM20 and MnSOD.

XANES. After cellular Mn mapping, a spectroscopic analysis (XANES) was performed to determine the oxidative state of Mn within subcellular compartments. Near edge absorption spectra of three control cells and of two cells overexpressing αSyn were recorded in the areas with the highest Mn concentrations (Figure 8A). In addition, the reference XANES spectra of Mn^{2+} and Mn^{4+} were collected. The analysis of the spectral shape and the edge positions of the XANES spectra revealed that cellular accumulations of Mn correspond to Mn^{2+} (Figure 8B) and that was the case in control cells as well as in cells overexpressing αSyn. Finally, extended X-ray beam exposure (three times 7 min per area during acquisition of XANES spectra) was performed in order to exclude sample degradation or radiation damages under cryogenic conditions. This analysis showed no changes of Mn spectra during prolonged X-ray exposition (data not shown).

Analysis of Mn Transport Proteins and Mn Release. In order to further explore the mechanisms of increased Mn content in αSyn overexpressing PMNs, we analyzed the expression of proteins involved in Mn import (VGCC and DMT1) and export (Fpn1). Western blot analyses showed no significant regulation of VGCC and DMT1, while there was a distinct trend to decreased Fpn1 levels at 3 days post-transfection. Thus, αSyn does not alter Mn import proteins, but may attenuate Mn export through Fpn1 (Figure 9A). On the other hand, αSyn contains at least one C-terminal binding site for Mn and therefore could act as an intracellular Mn store, hindering Mn from being exported.[17] To explore this hypothesis, PMN cultures, which were transfected to over-express αSyn or GFP, were treated with excess Mn. Three

DOI: 10.1021/acschemneuro.5b00093
ACS Chem. Neurosci. 2015, 6, 1769–1779

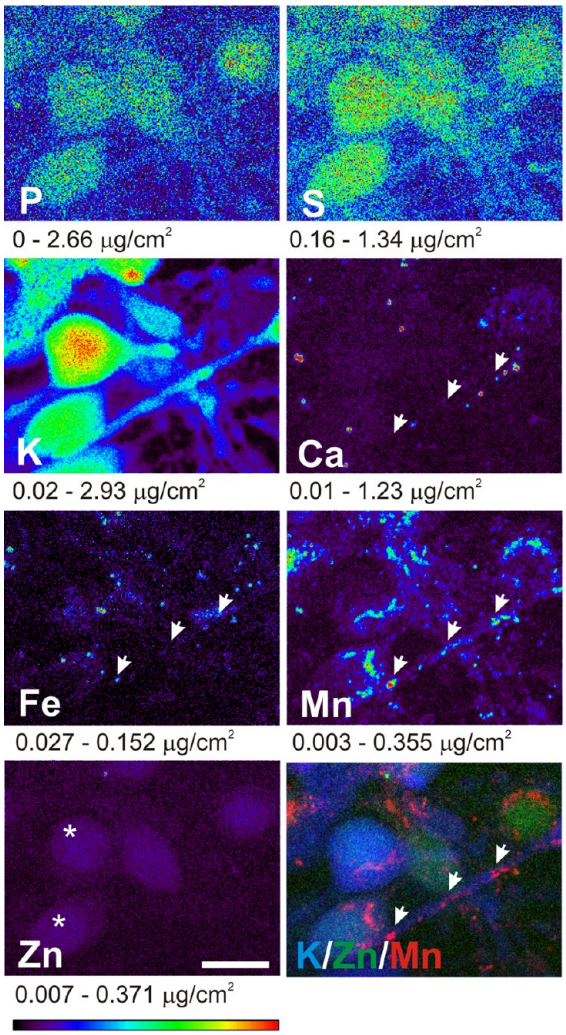

Figure 6. Elemental maps of primary midbrain neurons overexpressing αSyn treated with 500 μM Mn^{2+}. Representative XRF elemental maps of P, S, K, Ca, Fe, Mn, Zn, and a merged map of Mn/Zn/K imaged at cryogenic conditions at photon energy of 10 keV. Arrows point to Mn-rich foci, which partially are also enriched in Ca and/or Fe, in a clearly visualized neurite. Image size 41 × 32 $μm^2$, pixel size 150 nm, dwell time 250 ms. Rainbow scale corresponds to elemental concentrations in the ranges given below each scan. Asterisks (*) indicate two cells, which overexpress αSyn. Scale bar: 10 μm.

hours after Mn treatment, the medium was completely removed, cultures were gently washed with Mn-free medium (to remove any excess Mn) and Mn-free medium was added to the cultures. At 45 and 180 min after the Mn treatment, aliquots of the medium were taken and the Mn concentration was analyzed. Mn concentrations in the medium of αSyn-transfected cultures were significantly lower by 16.24 ± 2.74% (at 45 min) and 15.02 ± 1.57% (at 180 min) than in GFP-transfected control cultures (Figure 9B).

DISCUSSION

Transition metals are attributed an important role in the pathogenesis of neurodegenerative disorders. For example, accumulation of iron is well-known to occur in the substantia nigra in PD and exposure to Mn combined with other genetic and environmental factors can contribute to the development of Parkinsonism (reviewed in ref 18). αSyn is a natively unfolded protein, which aggregates and contributes to the formation of Lewy bodies in PD and in addition is known to interact with transition metals, such as Fe and Mn.[19] However, it remains an open question whether αSyn regulates the levels of transition metals in neuronal cells and if this regulation contributes to pathology observed in aggregopathies, such as PD. In this study, we therefore used synchrotron X-ray fluorescence to determine the spatial and quantitative distribution of Mn in rat primary midbrain neurons over-expressing αSyn. These analyses take advantage of the novel Bioprobe installed at the APS, which allows visualizing elemental maps of cryo-preserved specimens at an unprecedented resolution.[20] This permitted us to study the subcellular accumulation of Mn with higher spatial and chemical resolution than reported previously.[21]

Since the concentration of Mn in the culture medium is negligible, we supplemented the cell culture with Mn^{2+} to mimic environmental exposure to Mn. Control cultures without Mn supplementation showed only a very low intracellular Mn concentration (Figure 1), as was previously shown by our study.[21] In cells which were not treated with Mn, it was not possible to identify local cellular areas of higher concentrations. Several previous reports demonstrate localization of Mn inside of Mn-treated cells mainly focusing on mitochondria, the nucleus, or the Golgi apparatus,[22,23] respectively. In our experiment, in PMN cells cultures, which were supplemented with Mn, we observed a similar distribution in untransfected cells, where Mn was localized mainly in the cytoplasm in the perinuclear area. Interestingly, transfection with αSyn increased overall levels of Mn and its localization in the perinuclear area was even more pronounced (Figures 5 and 6). Previous reports showed that Mn treatment resulted in increased expression of αSyn.[24,25] Mn also increases the rate of αSyn fibrillation in vitro[26] and increased αSyn-aggregation was recently observed in the brain of *Cynomolgus macaques* after exposure to Mn.[27] Overexpression of αSyn in human cells seems to facilitate Mn-induced neurotoxicity through activation of the transcription factor NF-κB, the p38 MAPK kinase, and apoptotic signaling cascades, thus possibly playing a role in dopaminergic cell death.[28] Our results show a similar increase of cytotoxicity, when PMNs were both overexpressing αSyn and treated with excess Mn (Supporting Information Figure S2). Interestingly, overexpression of the PARK9 gene encoding for ATP13A2 protected from toxicity derived from αSyn-overexpression as well as from Mn exposure, thus suggesting a pathophysiological interaction of both factors.[29] Here we show, for the first time to our knowledge, a direct in situ visualization of increased Mn levels by overexpression of αSyn, suggesting that αSyn acts either as manganese store by binding and retaining the intracellular Mn or that it influences the transport of Mn into the cell. Consequently, we have shown that although overexpression of αSyn is not accompanied by a significant change in the expression of the most expressed proteins involved in Mn import (DMT1 and VGCC), there is a strong trend to less expression of Fpn1. Over time, this could result in increased intracellular Mn levels. Furthermore, Mn release was significantly attenuated by ∼20% in αSyn-overexpressing cultures. Since αSyn directly interacts and binds to Mn, we propose that it can act as an intracellular store for Mn.

High-resolution XRF imaging also permitted us to study the subcellular spatial distribution of all elements. In general, midbrain neurons showed mostly cytoplasmic localization of Mn, often in the perinuclear region with a polarized pattern: in neurons with a clearly identifiable neuritic process Mn was

DOI: 10.1021/acschemneuro.5b00093
ACS Chem. Neurosci. 2015, 6, 1769−1779

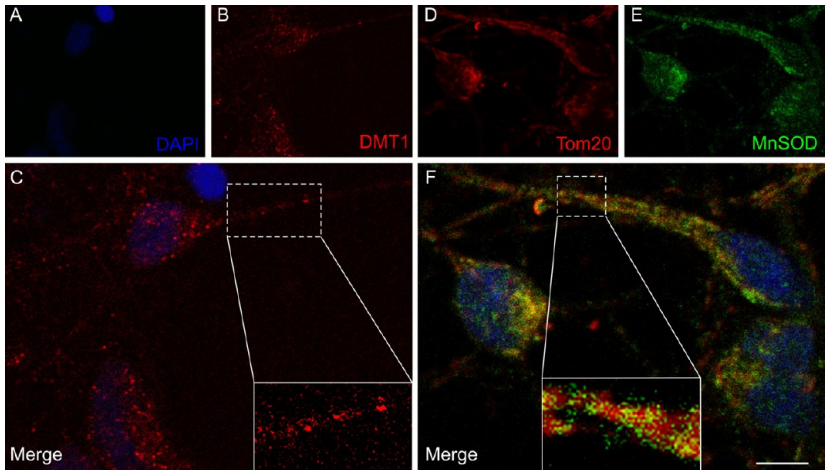

Figure 7. Subcellular distribution of DMT1 and MnSOD in primary midbrain neurons. Representative confocal microscopy image of a primary midbrain culture (immuno)stained for DAPI (A), DMT1 (B), and merge (C). Inset in (C) shows a magnification of DMT1 distribution in a neurite. Representative confocal microscopy image of a primary midbrain culture (immuno)stained for TOM20 (D), MnSOD (E), and merge of both with DAPI (F). Insets show a magnification of DMT1 (C) and TOM20/MnSOD (F) in a neurite. Scale bar: 5 μm.

especially prominent in the part of cytoplasm, which was oriented to the neurite. This distribution was previously described, and the Golgi apparatus was proposed as the site of principal Mn accumulation.[21,23,30] High levels of Mn were recently shown to exert neurotoxic effects in neurons through inhibition of the secretory pathway Ca^{2+}/Mn^{2+}-ATPase (SPCA) in the Golgi.[31] Our present examination resolves this distribution in significantly greater detail and also permitted us to clearly visualize Mn-rich foci in neuritic processes. These were of similar size as the Mn-rich areas of the cytoplasm and varied between a punctate/patchy and a filamentous appearance. Although a direct overlay of immunocytochemistry and X-ray fluorescence technically is not feasible, the comparison of Mn distribution and divalent metal transporter (DMT)1/MnSOD expression revealed a remarkable match. Since we did not detect much Mn outside of these structures, it is likely that a majority of the intracellular Mn is localized to cytoplasmic or neuritic DMT1 in organelles as well as in mitochondrial MnSOD. Previous reports demonstrated that Mn^{2+} is sequestered by brain mitochondria via the mitochondrial Ca^{2+} uniporter and is able to interfere there with F1ATPase and complex I-dependent oxidative phosphorylation.[32] This could result in a reduction of cellular viability and it is striking that in our measurements we find a significant and marked reduction of K in cells transfected with αSyn, which is an established finding in cells undergoing apoptosis.[33,34]

The levels of calcium in the cell are pivotal and tightly regulated since excess calcium may result in excitotoxicity and the induction of cell death. Our measurements show significant lower calcium levels in neurons transfected with αSyn (Figure 2). It has recently been shown that exposure to Mn^{2+} inhibits ATP-induced Ca entry into the cell by inhibition of the receptor-operated cation channel TRPC3.[35] Since αSyn increases intracellular levels of Mn, this effect could be more pronounced, resulting in lower Ca concentrations. On the other hand, Mn and Ca compete for the same channels, for example, voltage-gated Ca-channels (VGCC),[36] and an increased Mn influx could thus attenuate Ca entry by competition at these channels. As we previously showed, the expression of VGCC is higher in dopaminergic neurons of the midbrain, which could contribute to their selective vulnerability induced by Mn.[21]

Correlative studies of elemental levels can yield information on similarities in metabolism of specific elements. Because Mn, Ca, Mg, Fe, Cu, and Zn have similar ionic radii and valence states, they are known to mutually interact with each other's metabolic pathways.[37−39] Strikingly, we observed a strong correlation between Mn and Fe as well as Mn and Cu in αSyn-overexpressing neurons, that is, neurons with high concentrations of Mn also contained higher concentrations of Cu and Fe than neurons with lower Mn concentrations (Figure 3). Since an increase in intracellular Cu and Fe can be toxic,[40] increased levels of αSyn can by these means contribute to additional toxicity. In fact, the effect of Mn on Fe homeostasis has been previously implicated as one possible mechanism of Mn induced neurotoxicity.[41] Our data also supports the idea, that Mn, Cu and Fe employ similar entry mechanisms into the cell: one candidate could be the DMT1, which mediates the entry of a number of different divalent ions, that is, Mn, Fe, Cu, Zn, Pb, and Co. In dopaminergic neurons, DMT1 mediates Fe uptake and rats deficient for DMT1 are protected against iron-mediated neurotoxicity.[42] Interestingly, overexpression of DMT1 leads to increased dopaminergic cell death that is further aggravated by mutant αSyn,[43] which is supported by our data of increased Mn levels in αSyn overexpressing neurons. Based on the fact that aSyn has multiple binding sites for transition metals (reviewed in ref 44), our correlation analysis as well as the results from the Mn uptake and release studies suggest that aSyn acts as a molecular store for metals in the cell. Overexpression of αSyn did not seem to affect the levels of Cu, Cl, and Fe, and this stability underlines the differential regulation of Mn and Ca as specific effect induced by αSyn overexpression.

Our XANES results confirm that Mn is present in Mn^{2+} oxidation state and that this does not depend on αSyn expression. Since Mn^{3+} is unstable in aqueous solutions at pH > ~2 (unless stabilized by formation of stable complexes) and Mn^{4+} is usually encountered in insoluble complexes and particulate matter, Mn is likely to be present in this oxidation state (reviewed in ref 45). Overexpression of αSyn does not alter the redox state of Mn. Previous studies using XANES to determine the oxidation state of Mn complexes in brain mitochondria and neuron-like cells detected did not provide

DOI: 10.1021/acschemneuro.5b00093
ACS Chem. Neurosci. 2015, 6, 1769−1779

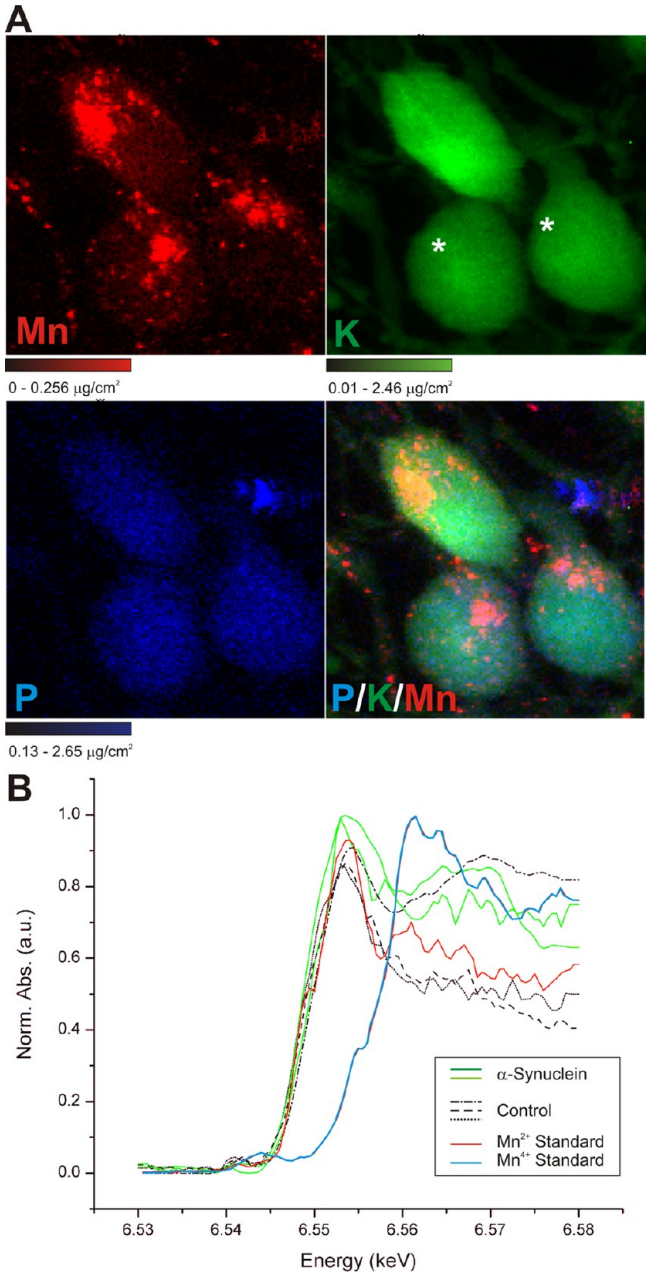

Figure 8. Determination of Mn oxidation states by XANES analysis. (A) Representative XRF maps of three typical primary midbrain neurons treated with 500 μM Mn^{2+}. Cells marked with an asterisk (*) overexpress αSyn. XRF maps of Mn (red), K (green), P (blue), and a merged map at 6.57 keV are shown. Image size 33 × 33 μm^2, pixel size 250 nm, dwell time 500 ms. The color scales correspond to elemental concentrations in the ranges given below each scan. (B) XANES analysis of Mn accumulates in neurons overexpressing αSyn (n = 2; green lines spectra) and control neurons (n = 3; black lines spectra). Spectra were acquired around the Mn edge at 6.545 keV in a typical Mn-rich area as shown in (A). Scans were performed with 0.5 eV steps with 3 s per point. Absorption spectra are shown as normalized absorption in arbitrary units. Reference spectra for Mn^{2+} (red line spectrum) and Mn^{4+} (blue line spectrum) are shown.

evidence for accumulation of any Mn^{3+} complex derived from oxidation of Mn^{2+}. However, the authors estimated that only small amounts of Mn^{3+} likely corresponding to spectra from Mn superoxide dismutase known to contain both Mn^{2+} and Mn^{3+}.[46]

In conclusion, our analyses demonstrate the distribution of Mn and other elements in primary midbrain neurons at a high spatial and chemical resolution. We also show that αSyn acts like an intracellular Mn store and alters the levels of intracellular Mn, Ca and other elements. On a longer time scale, similar alterations may contribute to chronic neurodegeneration in vivo. Therefore, therapeutic strategies targeting Mn import and regulating its homeostasis could represent an interesting therapeutic approach for future treatments of neurodegenerative disorders.

METHODS

Primary Midbrain Neuron (PMN) Culture, Transfection, and Mn Treatment. The mesencephalon floor of embryonic day 14 Wistar rats (bred in the central animal facility of the University of Göttingen) was dissected and dissociated for a primary cell culture as previously described.[47,48] Briefly, the brainstem was isolated and the meninges were removed. A medial incision was made at the ventricular opening of the tectum. The rostral parts of the ventral brainstem and of the tectum were cut away. The dissected tissue pieces were collected in ice-cold calcium−magnesium-free medium and centrifuged at 1.5g for 4 min. Trypsin (750 μL, 0.25%, Sigma, Taufkirchen, Germany) was added to the tissue pellet, and after 15 min of incubation at 37 °C was inactivated with 750 μL cold fetal calf serum. Dissociation of tissue fragments was achieved by gentle trituration using a fire-polished Pasteur pipet. The cell suspension was centrifuged at 73g for 4 min and resuspended in culture medium.

The cell suspension was then cotransfected with two plasmids, p.EGFP and p.αSyn-WT, which were previously described,[49,50] using nucleofection (Nucleofector II Device and Basic Primary Neurons Nucleofector Kit (VPI-1003), Lonza). For each experimental condition, a 90 μL cell suspension containing ∼4.0 × 10^6 neurons was nucleofected with 5 μg of plasmid DNA using the program O-05. Cells were then resuspended in culture medium containing DMEM-F12 (Invitrogen, Darmstadt, Germany) supplemented with 2.5 mg/mL BSA (35%), 0.9% D-(+)-glucose solution (45%), 2 mM L-glutamine (PAA Laboratories, Pasching, Austria), 5 μg/mL insulin, 1:100 N1 medium supplement, and 1:100 PSN antibiotic mixture (Invitrogen, Scotland, UK) and then plated at a density of 400 000/well on silicon nitride membranes (1.5 × 1.5 × 2 · 10^{-4} mm, Silson, U.K.) coated with poly-L-ornithine and laminin. Membranes were then transferred to 24-well plates (Saarstedt), and cells were kept in 500 μL of culture medium per well at 37 °C and 5% CO_2 in a humidified atmosphere. At 3 h after nucleofection, 2/3 of the medium was exchanged to discard toxic substances from the nucleofection procedure and 1/2 of the medium was exchanged again 48 h after plating. This midbrain culture contained ∼5−10% dopaminergic neurons and ∼90−95% GABAergic neurons with only single glial fibrillary acidic protein-positive cells being detectable.[51]

On day 3 in vitro, cultures were treated with Mn^{2+} (by supplementation with 500 μM $MnCl_2$; Sigma-Aldrich) for 2h in cell culture medium.

Fluorescence Light Microscopy in Vivo. All cultures were completely imaged using visible light microscopy (Axiovert; Zeiss), to create a localization map of the cells on the silicon nitride membrane and to identify GFP-positive DAergic neurons for subsequent X-ray imaging. Photomicrographs were taken using an inverted fluorescence microscope while the culture was kept in a heated (37 °C) imaging chamber under controlled atmosphere (5% CO_2). For each visual field, images at 10× magnification were taken using phase contrast and EGFP filter.

Sample Preparation for X-ray Microscopy. The sample preparation included preservation of the primary neurons by plunge freezing in liquid ethane. Samples were kept under cryogenic conditions and used for performing XRF and XANES measurements without freeze-drying. Previous experiments[21] have shown (i) best reproducibility and sensitivity of XRF, (ii) best preservation of elemental oxidation state by XANES, and (iii) minimal beam damage

DOI: 10.1021/acschemneuro.5b00093
ACS Chem. Neurosci. 2015, 6, 1769−1779

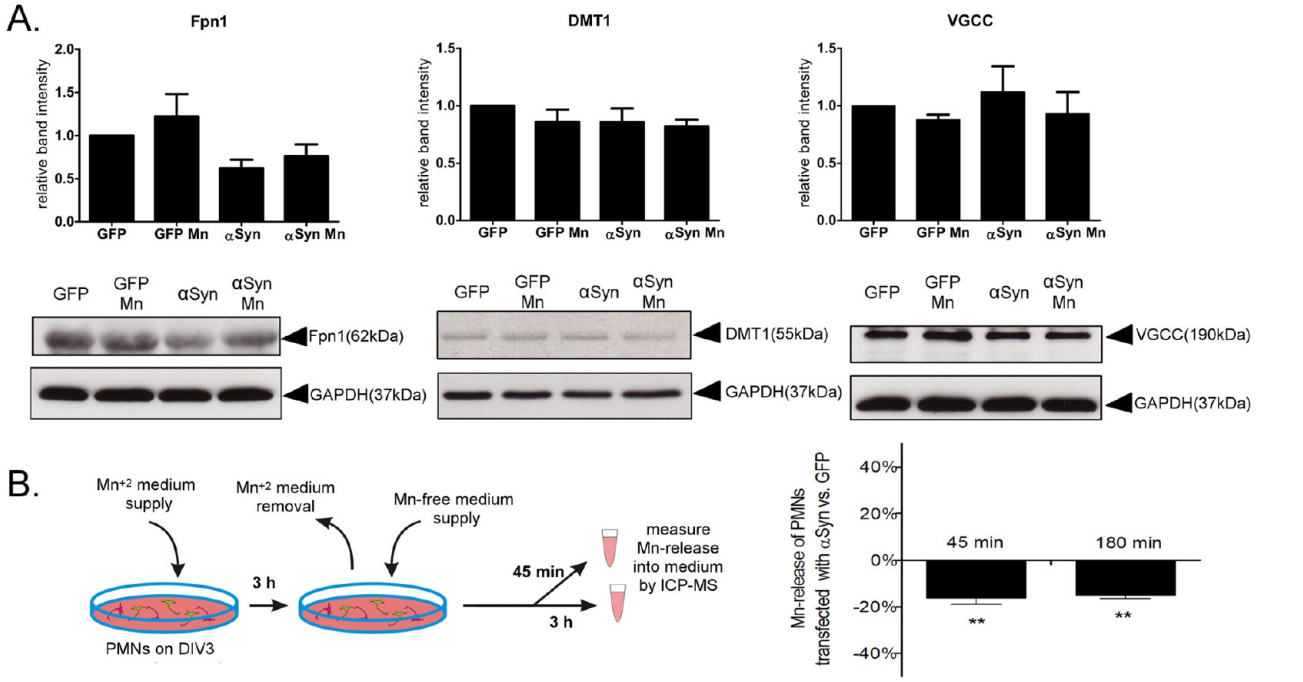

Figure 9. Analysis of Mn transport and Mn release. (A) Western blot analysis and quantification of the most expressed proteins for cellular trafficking of Mn (DMT1 and VGCC as Mn importers and Fpn1 as Mn exporter). One-way ANOVA did not reveal any significant differences between the different groups, but there was a clear trend for less Fpn1 expression in αSyn-treated cultures. (B) Left: Setup of Mn release experiment. Right: percentage of change in the release of Mn between cells transfected with αSyn and GFP (control). In αSyn-overexpressing cultures, the release of Mn into the culture medium was reduced as compared to GFP control transfected cells. $^{**}P < 0.01$ according to a one-sample t test.

when cells were analyzed in a frozen hydrated state. Imaging of frozen-hydrated cells under cryogenic conditions is a reliable way to preserve the structure of the cell and minimize rearrangement or loss of diffusible ions[52] as well as to minimize radiation damage.

Prior to plunge freezing, live-cells were thoroughly washed with fresh PBS buffer pH7.4 in order to remove excess extracellular metal ions. Subsequently, just prior to blotting, they were washed for 1 s in demineralized water to eliminate the PBS buffer. This method was chosen to remove the traces of inorganic ions. The cells prepared in this way were checked again under a visible light microscope to ensure that the morphology did not change after rinsing. Samples were quickly blotted for 1s with fine filter paper and immediately rapidly plunged in liquid ethane cooled with liquid nitrogen and subsequently stored under liquid nitrogen until imaging.

Prior to XRF imaging, frozen samples were examined under cryogenic conditions by using an optical fluorescence microscope (Nikon 50i) at the APS. The cryo-stage CLM77K (Instec, Inc.) mounted on the optical microscope allowed us to work at temperature of liquid nitrogen and to choose only those cells that are of highest interest for imaging with the X-ray microprobe. Detection of GFP-expressing cells helps to orient samples and later to identify the same transfected cells in the X-ray microscope for XRF and XANES measurements.

X-ray Microscopy. X-ray microscopy was performed at two instruments at the Advanced Photon Source (APS) at the Argonne National Laboratory. The X-ray fluorescence microscope at 2-ID-D is an instrument that allows cryogenic XANES and XRM studies at the K-absorption edge of Mn at 6539 eV combined with spatial resolution better than 200 nm and energy resolution of 0.5 eV. In addition, the 2-ID-D beamline allows imaging and spectroscopy measurements on frozen hydrated samples cooled by a cryo-jet (Oxford Instruments, UK), which preserves the physiological sample environment.

Furthermore, to determine the distribution of Mn within cells with the best possible sensitivity, we used the recently installed Bionanoprobe instrument located at APS-ANL at the Life Sciences-Collaborative Access Team sector 21-ID-D. The Bionanoprobe (BNP) is the first and only XFM instrument that allows imaging of frozen-hydrated biological samples up to 10−20 μm thickness, with an X-ray beam that can be focused to 30 nm.[20,53] The BNP is equipped with cryogenic capabilities and a robotic sample loading mechanism, which enables frozen-hydrated biological samples and other organic samples to be studied at ∼77 K. In this experiment, we used the nanofluorescence imaging to obtain distribution of trace metals with high spatial and chemical resolution at 10 keV, as well as to determine the colocalization of Mn with other trace elements such as Fe, Cu, and Zn. Usually the step size was 100 nm during the scanning, and dwell time 250 ms, with the focused beam flux of 3.5×10^9 photons/s. Spectra were collected on a pixel by pixel basis at 10 keV incident energy at the BNP, and 6.57 keV at 2-ID-D. The MAPS program was used for fitting and elements concentration analysis.[54] Thin film standards (NBS-1832/33) (The National Institute of Standards and Technology) and RF8-200-S2453 (AXO DRESDEN GmbH, Germany) were used at the 2-ID-D and the BNP, respectively, allowed for elemental quantification.

Immunohistochemistry for Confocal and Epifluorescence Microscopy. Coverslips with PMNs were fixed using 4% PFA for 10 min at 37 °C on DIV3. Permeabilization was performed using a solution of 0.3% Triton X-100 in PBS for 5 min followed by blocking with antibody diluent (Dako) for 20 min. For DMT1 staining, the coverslips were incubated with a primary DMT1 antibody (#NRAMP21-A, ADI) using a dilution of 1:100 in antibody diluent at 4 °C overnight. The secondary antibody, donkey anti-rabbit IgG conjugated with Alexa fluor 546 (#A10040, Invitrogen) diluted 1:1000 in antibody diluent, was applied for 15 min at 37 °C. For manganese superoxide dismutase (MnSOD) staining, a primary antibody against MnSOD (#06-984, Millipore) was applied at 4 °C overnight, the secondary antibody was a donkey anti-rabbit conjugated with Alexa fluor 680 (#A10043, Invitrogen) applied for 15 min at 37 °C. Then the primary antibody was saturated with fab fragment donkey anti-rabbit IgG (H+L) diluted 1:50 for 2 h (#711-007-003, Jackson lab). Subsequently, a primary antibody against TOM20 (#ab78547, abcam) diluted 1:50 was applied overnight at 4 °C, and the secondary antibody was donkey anti-rabbit IgG conjugated with Alexa fluor 546 (#A10040, Invitrogen) diluted 1:1000 in antibody diluent. Nuclei were stained

DOI: 10.1021/acschemneuro.5b00093
ACS Chem. Neurosci. 2015, 6, 1769−1779

using 4′,6-diamidine-2-phenylindole (DAPI; Sigma-Aldrich) for 5−10 min with a concentration of 1 μg/mL in PBS. Coverslips were mounted in Mowiol (Sigma-Aldrich), and confocal images were taken on a Leica TCS SP5.

For confirmation of αSyn-overexpression, we used a primary α-synuclein antibody (#610786, BD bioscience) at a dilution of 1:200 in antibody diluent at 4 °C overnight. The secondary antibody was a fab fragment goat-antimouse conjugated with Cy3 (#115165006, Dianova) using a dilution of 1:1000 in antibody diluent for 2 h. DAPI was then added for 5 min.

Western Blot and Solubility Assay. Western blots: Briefly, PMNs were lysed in ice-cold lysis buffer (10 mM HEPES, 142 mM KCl, 5 mM MgCl, 2.1 mM EGTA, IGEPAL, protease and phosphatase inhibitor and dithiothreitol) on DIV 3. Then samples were sonicated (Biorad) at 40% power for 15 s for 3 cycles on ice. Protein quantification was performed using a commercial BCA assay (Biorad) on a 96-well plate. Protein lysates were resolved on a 10% SDS-page and subsequently blotted on a polyvinylidene difluoride membrane. Aspecific binding was saturated by a solution of 5% nonfat powdered milk (Sigma-Aldrich) in TBS-Tween (50 mM Tris.HCl, pH 7.4, 150 mM NaCl, 0.1% Tween 20) at room temperature for 1 h. Incubations with primary anti-α-synuclein antibody (#610786, BD bioscience) dilution of 1:500, anti-DMT1 antibody (#NRAMP24-A, ADI) dilution of 1:100, anti-VGCC antibody (#C1103, Sigma) dilution of 1:200, and anti-Fpn1 antibody (#MTP11-S, ADI) dilution of 1:500 were performed overnight in 2.5% nonfat powdered milk. Incubation with primary anti-β-tubulin antibody (T4026, Sigma) and primary anti-GAPDH (#G9545, Sigma) both diluted 1:5000 were performed in 2.5% nonfat powdered milk for 1 h. The secondary antibody was a horseradish peroxidase-coupled IgG (Dianova, Hamburg, Germany) for both in a dilution of 1:5000 in 2.5% nonfat powdered milk and was applied for 1 h. For visualization, enhanced chemiluminescence (ECL-solution: 250 mM luminol, 90 mM *p*-coumaric acid, 1 M Tris/HCl, 30% hydrogen peroxide) was used. Blots were analyzed with ImageJ software (open freeware provided by the NIH, Bethesda, MD; http://imagej.nih.gov/ij/).

Solubility Assay. αSyn solubility was assessed as previously described.[55] For our experiments, H4 cells transfected with Synph-1/SynT were used as a positive control for aggregation. In short: cells were lysed in a lysis buffer (25 mM Tris pH 7.5, 150 mM NaCl, 1 mM EDTA and cocktail of protease inhibitors) and sonicated three times for 30 s on ice. Subsequently, 300 μg of total cell extracts was incubated with Triton X-100 (final concentration 1%) for 30 min. Then the soluble fraction was separated from the insoluble fraction by centrifuging for 1 h at 15 000*g* at 4 °C. The insoluble fraction was resuspended in the resuspension buffer (75 mM Tris, pH 6.8, 3% SDS, 15% glycerin, 3.75 mM EDTA pH 7.4, and a cocktail of protease inhibitors) and sonicated again for 15 s. Finally. Western blots were performed as described above.

Viability Assay. A commercial kit (ToxiLight BioAssay Kit by Lonza) was used for measuring the release of adenylate kinase from dead cells. At DIV3 after 3 h of Mn^{2+} incubation, an aliquot of cell medium for each condition was collected. Then the substrate was added to the 96-well plate and read with a Wallac 1450 MicroBeta TriLux instrument (PerkinElmer, Waltham, MA).

Manganese Determination by ICP-sf-MS Measurement. An ELEMENT 2, ICP-sectorfield-mass spectrometer (Thermo Scientific, Bremen, Germany) was employed for 55Mn determination in medium resolution mode. 103Rh was administered to each sample at a concentration of 1 μg/L as internal standard. Sample introduction was carried out using an ESI-Fast-system (Elemental Scientific, Mainz, Germany) connected to a Micromist nebulizer with a cyclon spray chamber. The RF power was set to 1200 W, the plasma gas was 15 L Ar/min, whereas the nebulizer gas was approximately 0.9 L Ar/min after daily optimization. Quality control for Mn determination: The determination methods had been validated previously by successful regular laboratory intercomparison studies, specifically as a reference laboratory for Mn determination in serum and urine of the GEQUAS quality control scheme and by regular analysis of adequate certified reference materials.

Statistical Analysis. For image and spectra analysis, we used MAPS, a freely available software for X-ray fluorescence analysis developed at the APS.[54] The algorithms employed are described in detail elsewhere.[56] Average of cellular element concentration was used after definition of single cell region of interest (ROIs) by using potassium map in the MAPS software. Data of elements concentration per cell are presented as means (±SE) of 18 transfected and 40 control cells, respectively. Statistical analyses of the data were performed using multivariate analysis of variance (ANOVA) and Pearson's correlative analysis in OriginLab 8-6 Pro software (Northampton, MA). Differences were considered significant with $P \leq 0.05$. For Western blot analyses, solubility assays and viability tests, at least three independent replicates were performed. One-way ANOVA followed by a Tukey posthoc test was then used to determine significances. For Mn release experiment analysis, we used a one-sample *t* test, assuming Mn-release of GFP-transfected cells as 100%.

■ ASSOCIATED CONTENT

Supporting Information

The Supporting Information is available free of charge on the ACS Publications website at DOI: 10.1021/acschemneuro.5b00093.

Overexpression of αSyn in primary midbrain neuron cultures; cytotoxicity of αSyn overexpression and Mn treatment; analysis of the solubility state of αSyn (PDF)

■ AUTHOR INFORMATION

Corresponding Authors

*E-mail: tducic@cells.es.
*E-mail: plingor@gwdg.de.

Author Contributions

[∇]T.D. and E.C. contributed equally to this work. T.D. and P.L. were involved with the conception, design of experiments, and interpretation of data. T.D., P.L., B.L., and S.C. performed the experiments at the synchrotron. T.D. and B.L. were involved with data analysis. E.C. performed confocal imaging, Western Blot analysis, and Mn release experiments. E.B. prepared cell cultures for all analyses. B.M. performed the mass spectrometry analysis for the Mn release experiment. D.F.L. and T.F.O. supplied the protocol for solubility analyses as well as H4 cell cultures. M.B. was overall supervising the research at the CNMPB. All authors contributed to the drafting and critical revision of the manuscript and have given final approval to the published version.

Funding

Use of the Advanced Photon Source, an Office of Science User Facility operated for the U.S. Department of Energy (DOE) Office of Science by Argonne National Laboratory, was supported by the U.S. DOE under Contract No. DE-AC02-06CH11357. The Cluster of Excellence and DFG Research Center for Nanoscale Microscopy and Molecular Physiology of the Brain (CNMPB) and the Deutsche Akademische Auslandsdienst (DAAD; PROCOPE program 2011) are acknowledged for financial support. T.D. was supported by CELLS ALBA in-house research grant "X-ray imaging of the protein aggregates induced by nanoparticles in vitro". P.L.'s work was funded by the Else Kröner-Fresenius-Stiftung.

Notes

The authors declare no competing financial interest.

DOI: 10.1021/acschemneuro.5b00093
ACS Chem. Neurosci. 2015, 6, 1769−1779

■ ACKNOWLEDGMENTS

We thank the Advanced Photon Source (APS) facility at the Argonne National Laboratory for beam time allocation (Proposal Id 29882) and excellent working conditions.

■ ABBREVIATIONS

αSyn, alpha synuclein; PD, Parkinson's disease; XRF, X-ray fluorescence; XANES, X-ray absorption near edge structure spectroscopy; PMN, primary midbrain neurons; BNP, Bionanoprobe; APS, Advanced Photon Source; MnSOD, manganese superoxide dismutase; DMT1, divalent metal transporter; Fpn1, ferroportin 1; VGCC, voltage-gated Ca-channels

■ REFERENCES

(1) Greger, J. L. (1999) Nutrition versus toxicology of manganese in humans: Evaluation of potential biomarkers. *NeuroToxicology 20*, 205−212.
(2) Guilarte, T. R. (2010) Manganese and Parkinson's disease: a critical review and new findings. *Environ. Health Perspect. 118*, 1071−1080.
(3) Pal, P. K., Samii, A., and Calne, D. B. (1999) Manganese neurotoxicity: A review of clinical features, imaging and pathology. *NeuroToxicology 20*, 227−238.
(4) Weintraub, D., Comella, C. L., and Horn, S. (2008) Parkinson's disease—Part 1: Pathophysiology, symptoms, burden, diagnosis, and assessment. *Am. J. Manag Care 14*, S40−8.
(5) Dexter, D., Carayon, A., Javoy-Agid, F., Agid, Y., Wells, F. R., Daniel, S. E., Lees, A. J., Jenner, P., and Marsden, C. D. (1991) Alterations in the levels of iron, ferritin and other trace metals in Parkinson's disease and other neurodegenerative diseases affecting the basal ganglia. *Brain 114*, 1953−1975.
(6) Gasser, T. (2007) Update on the genetics of Parkinson's disease. *Mov. Disord. 22*, S343−S350.
(7) Singleton, A. B., Farrer, M., Johnson, J., Singleton, A., Hague, S., Kachergus, J., Hulihan, M., Peuralinna, T., Dutra, A., Nussbaum, R., Lincoln, S., Crawley, A., Hanson, M., Maraganore, D., Adler, C., Cookson, M. R., Muenter, M., Baptista, M., Miller, D., Blancato, J., Hardy, J., and Gwinn-Hardy, K. (2003) alpha-Synuclein locus triplication causes Parkinson's disease. *Science 302*, 841−841.
(8) Lu, Y., Prudent, M., Fauvet, B., Lashuel, H. A., and Girault, H. H. (2011) Phosphorylation of α-Synuclein at Y125 and S129 alters its metal binding properties: implications for understanding the role of α-Synuclein in the pathogenesis of Parkinson's Disease and related disorders. *ACS Chem. Neurosci. 2*, 667−675.
(9) Kostka, M., Högen, T., Danzer, K. M., Levin, J., Habeck, M., Wirth, A., Wagner, R., Glabe, C. G., Finger, S., Heinzelmann, U., Garidel, P., Duan, W., Ross, C. A., Kretzschmar, H., and Giese, A. (2008) Single particle characterization of iron-induced pore-forming alpha-synuclein oligomers. *J. Biol. Chem. 283*, 10992−11003.
(10) HaMai, D., Campbell, A., and Bondy, S. C. (2001) Modulation of oxidative events by multivalent manganese complexes in brain tissue. *Free Radical Biol. Med. 31*, 763−768.
(11) Salditt, T., and Ducić, T. (2014) X-Ray Microscopy for Neuroscience: Novel Opportunities by Coherent Optics. In *Super-Resolution Microscopy Techniques in the Neurosciences*, pp 257−290, Humana Press, Totowa, NJ.
(12) Ducić, T., Quintes, S., Nave, K.-A., Susini, J., Rak, M., Tucoulou, R., Alevra, M., Guttmann, P., and Salditt, T. (2011) Structure and composition of myelinated axons: a multimodal synchrotron spectro-microscopy study. *J. Struct. Biol. 173*, 202−212.
(13) Ralle, M., and Lutsenko, S. (2009) Quantitative imaging of metals in tissues. *BioMetals 22*, 197−205.
(14) Ortega, R., Bohic, S., Tucoulou, R., Somogyi, A., and Devès, G. (2004) Microchemical element imaging of yeast and human cells using synchrotron X-ray microprobe with Kirkpatrick-Baez optics. *Anal. Chem. 76*, 309−314.
(15) McRae, R., Lai, B., Vogt, S., and Fahrni, C. J. (2006) Correlative microXRF and optical immunofluorescence microscopy of adherent cells labeled with ultrasmall gold particles. *J. Struct. Biol. 155*, 22−29.
(16) Roth, J., Ponzoni, S., and Aschner, M. (2013) Manganese homeostasis and transport. *Met Ions Life Sci. 12*, 169−201.
(17) Binolfi, A., Rasia, R. M., Bertoncini, C. W., Ceolin, M., Zweckstetter, M., Griesinger, C., Jovin, T. M., and Fernández, C. O. (2006) Interaction of alpha-synuclein with divalent metal ions reveals key differences: a link between structure, binding specificity and fibrillation enhancement. *J. Am. Chem. Soc. 128*, 9893−9901.
(18) Paris, I., and Segura-Aguilar, J. (2012) The role of metal ions in dopaminergic neuron degeneration in Parkinsonism and Parkinson's disease. In *Metal Ions in Neurological Systems*, pp 31−39, Springer, Vienna, Vienna.
(19) Binolfi, A., Rodriguez, E. E., Valensin, D., D'Amelio, N., Ippoliti, E., Obal, G., Duran, R., Magistrato, A., Pritsch, O., Zweckstetter, M., Valensin, G., Carloni, P., Quntanar, L., Griesinger, C., and Fernández, C.O. (2010) Bioinorganic chemistry of Parkinson's disease: structural determinants for the copper-mediated amyloid formation of alpha-synuclein. *Inorg. Chem. 49*, 10668−79.
(20) Yuan, Y., Chen, S., Paunesku, T., Gleber, S. C., Liu, W. C., Doty, C. B., Mak, R., Deng, J., Jin, Q., Lai, B., Brister, K., Flachenecker, C., Jacobsen, C., Vogt, S., and Woloschak, G. E. (2013) Epidermal growth factor receptor targeted nuclear delivery and high-resolution whole cell X-ray imaging of Fe3O4@TiO2 nanoparticles in cancer cells. *ACS Nano 7*, 10502−10517.
(21) Ducić, T., Barski, E., Salome, M., Koch, J. C., Bähr, M., and Lingor, P. (2013) X-ray fluorescence analysis of iron and manganese distribution in primary dopaminergic neurons. *J. Neurochem. 124*, 250−261.
(22) Kalia, K., Jiang, W., and Zheng, W. (2008) Manganese accumulates primarily in nuclei of cultured brain cells. *NeuroToxicology 29*, 466−470.
(23) Carmona, A., Devès, G., Roudeau, S., Cloetens, P., Bohic, S., and Ortega, R. (2010) Manganese Accumulates within Golgi Apparatus in Dopaminergic Cells as Revealed by Synchrotron X-ray Fluorescence Nanoimaging. *ACS Chem. Neurosci. 1*, 194−203.
(24) Cai, T., Yao, T., Zheng, G., Chen, Y., Du, K., Cao, Y., Shen, X., Chen, J., and Luo, W. (2010) Manganese induces the overexpression of α-synuclein in PC12 cells via ERK activation. *Brain Res. 1359*, 201−207.
(25) Li, Y., Sun, L., Cai, T., Zhang, Y., Lv, S., Wang, Y., and Ye, L. (2010) alpha-Synuclein overexpression during manganese-induced apoptosis in SH-SY5Y neuroblastoma cells. *Brain Res. Bull. 81*, 428−433.
(26) Uversky, V. N., Li, J., and Fink, A. L. (2001) Metal-triggered structural transformations, aggregation, and fibrillation of human alpha-synuclein. A possible molecular NK between Parkinson's disease and heavy metal exposure. *J. Biol. Chem. 276*, 44284−44296.
(27) Verina, T., Schneider, J. S., and Guilarte, T. R. (2013) Manganese exposure induces α-synuclein aggregation in the frontal cortex of non-human primates. *Toxicol. Lett. 217*, 177−183.
(28) Bowman, A. B., Kwakye, G. F., Herrero Hernández, E., and Aschner, M. (2011) Role of manganese in neurodegenerative diseases. *J. Trace Elem. Med. Biol. 25*, 191−203.
(29) Gitler, A. D., Chesi, A., Geddie, M. L., Strathearn, K. E., Hamamichi, S., Hill, K. J., Caldwell, K. A., Caldwell, G. A., Cooper, A. A., Rochet, J.-C., and Lindquist, S. (2009) α-Synuclein is part of a diverse and highly conserved interaction network that includes PARK9 and manganese toxicity. *Nat. Genet. 41*, 308−315.
(30) Carmona, A., Roudeau, S., Perrin, L., Veronesi, G., and Ortega, R. (2014) Environmental manganese compounds accumulate as Mn(ii) within the Golgi apparatus of dopamine cells: relationship between speciation, subcellular distribution, and cytotoxicity. *Metallomics 6*, 822.
(31) Sepúlveda, M. R., Wuytack, F., and Mata, A. M. (2012) High levels of Mn 2+inhibit secretory pathway Ca 2+/Mn 2+-ATPase (SPCA) activity and cause Golgi fragmentation in neurons and glia. *J. Neurochem. 123*, 824−836.

DOI: 10.1021/acschemneuro.5b00093
ACS Chem. Neurosci. 2015, 6, 1769−1779

(32) Gavin, C. E., Gunter, K. K., and Gunter, T. E. (1999) Manganese and calcium transport in mitochondria: implications for manganese toxicity. *NeuroToxicology 20*, 445−453.
(33) Fernández-Segura, E., Cañizares, F. J., Cubero, M. A., Warley, A., and Campos, A. (1999) Changes in Elemental Content During Apoptotic Cell Death Studied by Electron Probe X-Ray Microanalysis. *Exp. Cell Res. 253*, 454−462.
(34) Ramos, J. M., Arrebola, F., Fernandez-Cervilla, F. J., Crespo, V., and Fernandez-Segura, E. (2011) Electron probe X-ray microanalysis of cisplatin-induced cell death in rat pheochromocytoma PC12 cells. *Histol. Histopathol. 26*, 333−342.
(35) Streifel, K. M., Miller, J., Mouneimne, R., and Tjalkens, R. B. (2013) Manganese inhibits ATP-induced calcium entry through the transient receptor potential channel TRPC3 in astrocytes. *Neuro-Toxicology 34*, 160−166.
(36) Narita, K., Kawasaki, F., and Kita, H. (1990) Mn and Mg influxes through Ca channels of motor nerve terminals are prevented by verapamil in frogs. *Brain Res. 510*, 289−295.
(37) Drapeau, P., and Nachshen, D. A. (1984) Manganese fluxes and manganese-dependent neurotransmitter release in presynaptic nerve endings isolated from rat brain. *J. Physiol. 348*, 493.
(38) Fitsanakis, V. A., Zhang, N., Garcia, S., and Aschner, M. (2010) Manganese (Mn) and iron (Fe): interdependency of transport and regulation. *Neurotoxic. Res. 18*, 124−131.
(39) Kwik-Uribe, C. L., Reaney, S., Zhu, Z., and Smith, D. (2003) Alterations in cellular IRP-dependent iron regulation by in vitro manganese exposure in undifferentiated PC12 cells. *Brain Res. 973*, 1−15.
(40) Jomova, K., Vondrakova, D., Lawson, M., and Valko, M. (2010) Metals, oxidative stress and neurodegenerative disorders. *Mol. Cell. Biochem. 345*, 91−104.
(41) Fernsebner, K., Zorn, J., Kanawati, B., Walker, A., and Michalke, B. (2014) Manganese leads to an increase in markers of oxidative stress as well as to a shift in the ratio of Fe(ii)/(iii) in rat brain tissue. *Metallomics 6*, 921−931.
(42) Salazar, J., Mena, N., Hunot, S., Prigent, A., Alvarez-Fischer, D., Arredondo, M., Duyckaerts, C., Sazdovitch, V., Zhao, L., Garrick, L. M., Nuñez, M. T., Garrick, M. D., Raisman-Vozari, R., and Hirsch, E. C. (2008) Divalent metal transporter 1 (DMT1) contributes to neurodegeneration in animal models of Parkinson's disease. *Proc. Natl. Acad. Sci. U. S. A. 105*, 18578−18583.
(43) Chew, K. C. M., Ang, E.-T., Tai, Y. K., Tsang, F., Lo, S. Q., Ong, E., Ong, W.-Y., Shen, H.-M., Lim, K.-L., Dawson, V. L., Dawson, T. M., and Soong, T. W. (2011) Enhanced autophagy from chronic toxicity of iron and mutant A53T α-synuclein: implications for neuronal cell death in Parkinson disease. *J. Biol. Chem. 286*, 33380−33389.
(44) Carboni, E., and Lingor, P. (2015) Insights on the interaction of alpha-synuclein and metals in the pathophysiology of Parkinson's disease. *Metallomics 7*, 395−404.
(45) Martinez-Finley, E. J., Gavin, C. E., Aschner, M., and Gunter, T. E. (2013) Manganese neurotoxicity and the role of reactive oxygen species. *Free Radical Biol. Med. 62*, 65−75.
(46) Gunter, K. K., Aschner, M., Miller, L. M., Eliseev, R., Salter, J., Anderson, K., and Gunter, T. E. (2006) Determining the oxidation states of manganese in NT2 cells and cultured astrocytes. *Neurobiol. Aging 27*, 1816−1826.
(47) Knöferle, J., Ramljak, S., Koch, J. C., Tönges, L., Asif, A. R., Michel, U., Wouters, F. S., Heermann, S., Krieglstein, K., Zerr, I., Bähr, M., and Lingor, P. (2010) TGF-beta 1 enhances neurite outgrowth via regulation of proteasome function and EFABP. *Neurobiol. Dis. 38*, 395−404.
(48) Shimoda, K., Sauve, Y., Marini, A., Schwartz, J. P., and Commissiong, J. W. (1992) A high percentage yield of tyrosine hydroxylase-positive cells from rat E14 mesencephalic cell culture. *Brain Res. 586*, 319−331.
(49) Taschenberger, G., Garrido, M., Tereshchenko, Y., Bähr, M., Zweckstetter, M., and Kügler, S. (2012) Aggregation of αSynuclein promotes progressive in vivo neurotoxicity in adult rat dopaminergic neurons. *Acta Neuropathol. 123*, 671−683.
(50) Koch, J. C., Barski, E., Lingor, P., Bähr, M., and Michel, U. (2011) Plasmids containing NRSE/RE1 sites enhance neurite outgrowth of retinal ganglion cells via sequestration of REST independent of NRSE dsRNA expression. *FEBS J. 278*, 3472−3483.
(51) Lingor, P., Unsicker, K., and Krieglstein, K. (2000) GDNF and NT-4 Protect Midbrain Dopaminergic Neurons from Toxic Damage by Iron and Nitric Oxide. *Exp. Neurol. 163*, 55−62.
(52) Zierold K. Cryotechniques for biological microanalysis. In *Microbeam Analysis*; Russel, P. E., Ed.; San Francisco Press Inc.: San Francisco, CA, 1989pp 109−11
(53) Chen, S., Deng, J., Yuan, Y., Flachenecker, C., Mak, R., Hornberger, B., Jin, Q., Shu, D., Lai, B., Maser, J., Roehrig, C., Paunesku, T., Gleber, S. C., Vine, D. J., Finney, L., Vonosinski, J., Bolbat, M., Spink, I., Chen, Z., Steele, J., Trapp, D., Irwin, J., Feser, M., Snyder, E., Brister, K., Jacobsen, C., Woloschak, G., and Vogt, S. (2014) The Bionanoprobe: hard X-ray fluorescence nanoprobe with cryogenic capabilities. *J. Synchrotron Radiat. 21*, 66−75.
(54) Vogt, S. (2003) MAPS: A set of software tools for analysis and visualization of 3D X-ray fluorescence data sets. *J. Phys. IV 104*, 635−638.
(55) Lázaro, D. F., Rodrigues, E. F., Langohr, R., Shahpasandzadeh, H., Ribeiro, T., Guerreiro, P., Gerhardt, E., Kröhnert, K., Klucken, J., Pereira, M. D., Popova, B., Kruse, N., Mollenhauer, B., Rizzoli, S. O., Braus, G. H., Danzer, K. M., and Outeiro, T. F. (2014) Systematic comparison of the effects of alpha-synuclein mutations on its oligomerization and aggregation. *PLoS Genet. 10*, e1004741.
(56) Vogt, S., Maser, J., and Jacobsen, C. (2003) Data analysis for X-ray fluorescence imaging. *J. Phys. IV 104*, 617−622.

DOI: 10.1021/acschemneuro.5b00093
ACS Chem. Neurosci. 2015, 6, 1769−1779